JOURNAL OF AIRCRAFT
Vol. 30, No. 4, July–Aug. 1993

Zero-Thrust Glide Testing for Drag and Propulsive Efficiency of Propeller Aircraft

Jack Norris*
Management Consultant, Northridge, California 91326
and
Andrew B. Bauer†
Douglas Aircraft Company, Orange, California 92667

The authors have developed a new method, "zero-thrust glide testing," that provides the first really practical, accurate, and inexpensive method for measuring the drag of propeller aircraft in gliding flight. Zero-thrust conditions were sensed on a classic Luscombe 8E by monitoring the fore and aft clearance motion of the engine crankshaft as the engine rpm or power was changed. With zero engine thrust conditions, gliding flight measurements were made to find the drag polar and propeller airfoil zero-lift angles. The glide polar and level flight measurements have been used to find the propulsive efficiency. The airfoil zero-lift angles were used to accurately calculate the propeller thrust, and therefore, the drag in powered level flight. Drag in level flight cruise is approximately 30% larger than in glide, resulting in a propulsive efficiency equal to 0.62. Propeller efficiency has been calculated using standard methods corrected for the interference between the propeller and the airframe flowfields. The interference changed the propeller thrust, created an inviscid buoyancy drag on the fuselage, and generated viscous-related drag forces. The viscous forces and engine cooling duct losses are the cause for the poor propulsive efficiency and are believed to be typical of many propeller-driven aircraft.

Introduction

IN 1982 the authors set out to find a practical and accurate method for obtaining the true, full-scale drag levels and propulsion efficiency of propeller-driven aircraft. The objective was to use flight test measurements only, independent of any theoretical analysis. The motivation for this work was the belief that 1) the propulsion efficiency of typical aircraft in cruising conditions is far different from that of a nominal 80% propeller efficiency, but that 2) there had been no practical way to get factual, full-scale data. The typical propulsive efficiency, using an 80% propeller efficiency, is evidently near 60% because of the extra drag losses that come with typical engine and propeller installations. The interference drag between the propeller wake and the rest of the airframe is significant. The engine cooling drag is significant. Since the large losses associated with engine and propeller installations are not generally recognized, the authors began the development of a method to measure and expose such losses.

In 1989, after seven years of testing and analysis to investigate the problem, the authors developed the zero-thrust glide testing method for determining gliding drag and propulsive efficiency. The method was developed using the first author's classic Luscombe 8E as a test vehicle. A three-view drawing of the Luscombe is shown in Figure 1. The measured propulsive efficiency is very poor, near 62% at cruising speeds, which is corroborated by the 58% efficiency found by Raspet and Lambros[1] using a propellerless Bellanca aircraft with sealed engine cooling ducts and towed-up for glide testing. An analysis of the propulsive efficiency problem has been developed to show the source of the problems that need to be overcome in order to develop more efficient propeller aircraft.

The zero-thrust method is based on a very simple but technically significant thrust switch. The switch was designed to have a high natural frequency so as to be invulnerable to engine vibration. The small fore and aft motion of the engine crankshaft is sensed as the aircraft is flown in a steady glide with the engine rpm or power adjusted to stay accurately at "zero-thrust" or at an accurately-known bias thrust. A crankshaft is free to move in the axial direction, affected only by the propeller thrust and the inclined weight components of the crankshaft and the propeller assembly. Rotating engine crankshifts generally do not have significant axial friction forces, gear forces, or pressure-biasing forces. The vented crankcase pressure is very close to atmospheric pressure. The engine thrust bearings allow the shaft to "float," providing no significant axial forces. When the aircraft is gliding at the speed where the crankshaft is level, only the propeller thrust is significant for affecting the small fore and aft motion that the shaft thrust bearings allow.

Raspet and Lambros[1] found that the drag of the Bellanca increased significantly when the sealed engine cooling ducts were opened. Johnson[2,3] has developed sailplane sink rate and drag measurement testing to a high degree of perfection, showing small hills or valleys in drag curves as turbulent flow

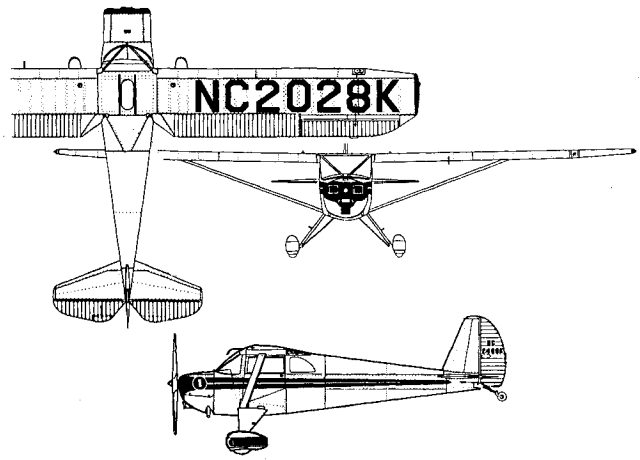

Fig. 1 Three-view drawing of the Classic Luscombe 8E.

Presented as Paper 90-0233 at the AIAA 28th Aerospace Sciences Meeting, Reno, NV, Jan. 8–11, 1990; received Oct. 6, 1990; revision received May 5, 1992; accepted for publication May 27, 1992.

*11613 Seminole Circle.
†Retired, 627 Monroe Avenue. Associate Fellow AIAA.

or separation phenomena occur. For these references and the present work, drag is found from the flight mechanics relation

$$D = T + (WV_S/V) \quad (1)$$

where W is the weight, V_S is the sinking speed, V is the true airspeed, T is thrust, and D is drag. Drag is readily obtained when the thrust is zero, since W, V_S, and V can be obtained using ground and flight measurements.

Thrust is included in Eq. (1) to make it applicable to cases where thrust is not zero.

In marked contrast to propeller removal and towing to find glide drag, zero-thrust glide testing has great practical benefits. It is more safe and eliminates the costs and inconvenience of a tow plane. Secondly, it enables the aircraft to do many glide runs during a single flight, as the engine can be used to regain the altitude lost during a glide. Thirdly, and most significantly, the testing area can be remote from the airfield, since the return to the airfield is not limited to gliding flight. The area can be chosen so as to minimize the undesired effects of updrafts, downdrafts, or unstable air. We found dawn testing over the stable ocean ideal for producing high-quality data.

The procedures for zero-thrust testing depend on the aircraft propeller type. For aircraft with a fixed-pitch propeller, such as the Luscombe, the ratio of engine rpm to true airspeed can be measured at the glide speed where the crankshaft is level. This ratio can be used as a calibration to determine the rpm for testing at all airspeeds. The use of the ratio insures that all test points are done with a propeller thrust very close to zero, as shown later.

A second testing procedure can be applied to aircraft with either a fixed-pitch or a variable-pitch, constant-speed propeller. This can be done at any airspeed by taking into account the effects of 1) the sum of the crankshaft weight and the propeller weight, W_{CP} [47 lb (209 N) on the Luscombe], and 2) the measured inclination of the crankshaft, θ_{t1}, where θ_{t1} is positive for a nose-up shaft inclination. Then the zero-thrust or crankshaft position sensor is used to set the thrust equal to $W_{CP} \sin \theta_{t1}$. This thrust bias is used in Eq. (1) to determine the corresponding drag, which is called D_{TS}, the drag using the thrust sensor. Since airplane drag varies with the thrust level, D_{TS} is somewhat different from D_G, the drag for gliding (zero-thrust) flight. An interpolation, using both the level-flight drag, D_L (discussed below), and D_{TS} can be used to find D_G. The difference between D_{TS} and D_G is generally very small.

Propulsive efficiency η_P is defined as the ratio of the ideal power required to fly the airplane divided by the actual engine power used in level flight conditions, P_L. The ideal power is defined as the airspeed V times the gliding drag D_G with the lift equal to the weight. Hence, the efficiency is

$$\eta_P = D_G V/P_L = D_G/D_{EP} \quad (2)$$

where D_{EP}, the "drag equivalent to engine power" is given by P_L/V. The engine power may be determined by any one of three methods: 1) the use of measured flight conditions with engine-manufacturers power charts; 2) the calculation of propeller power; or 3) the direct measurement of engine torque and RPM. The first two methods are used in this article, and the third method is under development.

This article addresses the low propulsive efficiency problem, which has not been addressed well because there has not been a practical test method to identify it. The problem is in the interaction of the propeller slipstream with the rest of the aircraft.

First, consider the fact that the presence of the fuselage or airframe changes the airspeed in the propeller plane. The airspeed change, discussed by Glauert,[4] causes an inviscid buoyancy thrust (or drag) on the airframe. The sum of the buoyancy force T_B and the direct thrust force on the propeller T_P is called the "total thrust" T. The total thrust rather than the direct thrust is used to define the propeller efficiency η. The work of Glauert[4] and methods of Larrabee,[5,6] and Adkins and Liebeck[7] have been combined in a program for calculating buoyancy thrust, direct thrust, and propeller efficiency.

Secondly, the slipstream viscous effects increase the drag in level flight D_L to a value that may be as much as 35% higher than that in the glide. The ratio D_G/D_L is defined as the level flight efficiency factor η_L. The propeller efficiency η is given by D_L/D_{EP}. Therefore, we have the definitions

$$\eta_P = (D_G/D_L)(D_L/D_{EP}) = \eta_L \eta \quad (3)$$

The program for calculating thrust is sensitive to the propeller pitch angles and to the propeller airfoil angles of zero lift. This problem is overcome by using the program to find zero-lift angles that agree with the glide test results. Then the program is useful for accurate calculations of both the power input into the propeller and propeller efficiency. Then D_L may be obtained from

$$D_L = \eta D_{EP} = \eta P_L/V \quad (4)$$

Luscombe 8E Flight Test Operation and Data Collection

The Luscombe 8E is an appropriate, classic test vehicle for developing the zero-thrust test method. The vehicle has been owned by the first author for 40 yr and has been maintained in "like new" condition. The aircraft was operated from the Camarillo, California airport during the test program. All the level flight testing was done at 800-ft pressure altitude over the surveyed, 11,100-ft-long former military runway. The level flight results were used to accurately calibrate the pitot-static airspeed system. This was done by a series of upwind and downwind runs in calm, evening air. The tachometer and the altimeter were laboratory calibrated.

For the glide test program, a simple and rugged thrust switch was fabricated by attaching a short piece of 0.062-in. (1.59-mm) diam music wire to a small, insulating phenolic block. The block was rigidly bolted to the crankcase so that the tip of the wire just touched the crankshaft flange as the crankshaft was moved halfway through the fore and aft travel range, nominally 0.010 in. (0.25 mm). A light-emitting diode was used for a positive indication as to whether or not the tip was touching the crankshaft flange. The wire was configured to have a very high natural frequency, and thus was insensitive to engine vibration frequency. These procedures were necessary to get a valid measurement of the small crankshaft motion in a high-vibration environment.

Glide testing was done in the stable dawn and dusk air over the Pacific Ocean near Ventura, California. The runs were made between 3000–2000-ft pressure altitude. The altimeter calibration was checked using a nearby 3111-ft coastal mountain survey peak and the known altitude of the Camarillo airport runway. Temperature effects were accounted for in the calibration and during all the flight testing. An equivalent airspeed of 67.2 mph (30.04 m/s) was required to keep the crankshaft level in gliding flight at the test weight, and the zero-thrust sensor was used to find that zero thrust was obtained using 14.94 rpm per mph (33.42 rpm per m/s) of true airspeed. All testing runs were repeated several times to check that the data were accurate.

Repetition was especially useful for the glide runs, which required maintaining constant airspeed, constant engine rpm, and carefully timing the descent through the nominal 1000-ft altitude change. The selected altitude change was large enough for accurate timing of the descent, and small enough that the effects of air density changes on true airspeed and flight dynamics could be handled. Data calculations were done using the mean altitude. Stable dawn air over the ocean proved to be an ideal way to obtain consistent and accurate data.

Tables 1 and 2 give the measured data, which has been corrected using the instrument calibration curves.

Table 1 Glide data

W, lb	rpm	EAS, mph	Temperature, °F	Sink time, s
1192.6	822	51.5	82	126.58
1267.0	969	61.0	76	125.55
1183.7	1054	66.0	82	119.52
1258.2	1123	70.7	76	112.13
1227.9	1284	80.55	80	91.62
1231.3	1447	90.75	80	72.48
1216.4	1579	100.1	81	57.56
1204.3	1773	111.0	82	42.20

Table 2 Level flight data

W, lb	rpm	EAS, mph	Density, slugs/ft³	Temperature, °F	Manifold press, in. Hg
1242.8	1650	57.36	0.002244	74	18.5
1253.8	1650	63.22	0.002244	74	18.5
1248.8	1760	71.28	0.002244	74	19.2
1289.0	1860	77.73	0.002260	70	20.3
1298.3	1970	85.59	0.002260	70	21.4
1282.8	2070	89.56	0.002260	70	22.3
1275.6	2175	94.20	0.002260	70	23.5
1269.2	2280	99.42	0.002260	70	24.8
1262.6	2380	105.71	0.002260	70	26.0
1258.6	2540	111.26	0.002244	74	28.0

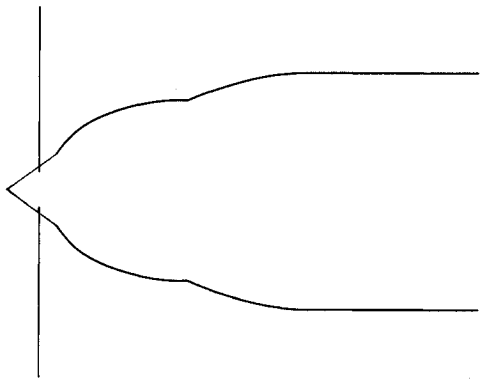

Fig. 2 Propeller plane and the Luscombe 8E fuselage profile.

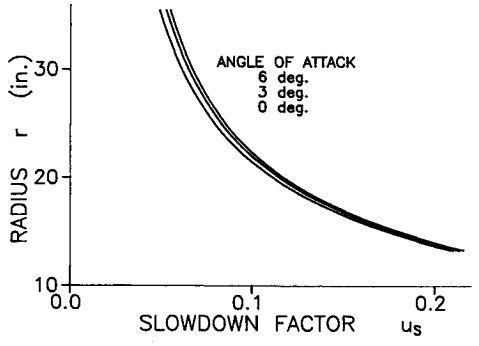

Fig. 3 Luscombe 8E airspeed slowdown factor at the propeller plane.

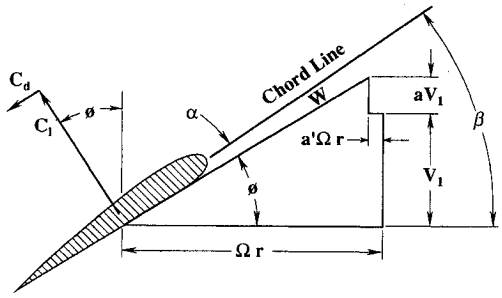

Fig. 4 Parameters used to define the velocity vector W with respect to a propeller airfoil section.

Calculation of Airstream Slowing at the Propeller Plane

The fuselage and other parts of an airframe affect the local airspeed at the propeller plane. For a tractor aircraft such as the Luscombe, the change is generally a slowing of the stream. In order to investigate the slowing for the Luscombe, the fuselage cross-sectional area distribution was measured and plotted as a function of the distance behind the propeller quarter chord. The area was converted to the equivalent radius and plotted as a function of the distance, as shown on Fig. 2. This shape was matched by a computer program having a source-sink distribution along the axis. The distribution was used to calculate the slowing of the airstream in the propeller plane. Effects of the noncircular fuselage cross section were neglected. A significant amount of the slowing is the result of the area increase from the windshield, which starts about 28 in. from the propeller plane.

The axial airspeed in the propeller plane with the propeller removed was defined as $V_1(r)$, where r is the radius from the fuselage axis. $V_1(r)$ was expressed as

$$V_1(r) = V_0[1 - u_s(r)] \tag{5}$$

where V_0 is the freestream speed and $u_s(r)$ is defined as the "slowdown factor."

Two much smaller slowing phenomena are those from the wing volume and the airplane wake. These together were calculated to slow the propeller airstream by a factor averaging 0.0162 over the propeller plane.

Another small slowdown effect is generated by the wing circulation, which varies with the airplane angle of attack and wing lift coefficient. At a lift coefficient of 0.3 the effect was calculated to slow the stream by a factor of 0.0063.

The total propeller plane slowing caused by the four phenomena was assumed to be given to a good approximation by addition. The sum is plotted as $u_s(r)$ on Fig. 3. The fuselage effect is largest near the propeller hub and much smaller at the propeller tips. The average effect for the whole propeller was a slowing factor near 0.085.

Propeller Performance and the Interaction of the Slipstream with the Airframe

The calculation of propeller performance in a uniform freestream has been addressed by Larrabee[5,6] and by Adkins and Liebeck.[7] The method uses annular stream tubes to calculate the parameters shown on Fig. 4 for any station at radius r along the propeller blades, and the blade forces are integrated to determine thrust, torque, and propeller efficiency. Appendix A outlines a method for solving for the unknown coefficients a and a', the axial and rotational induced airspeed factors, as a function of r, the blade element radius. When a and a' are determined, the calculation of the velocity vector $W(r)$ and the blade force coefficients $c_l(r)$ and $c_d(r)$ is a straightforward matter.

Effects of adding a body of revolution into the freestream and propeller flowfield are illustrated on Fig. 5. The four solid lines surrounding the body represent streamlines from two annular stream tubes for the case where the propeller thrust is zero. When the propeller rpm or speed is increased, thrust is produced, and the stream tubes move inward as shown by the dashed lines.

First, consider the inviscid features of the flow, those outside the boundary layer on the body. The buoyancy thrust

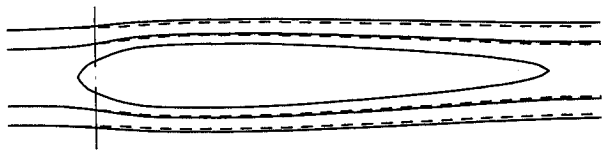

Fig. 5 Cross-sectional view of a body surrounded by two annular stream tubes.

comes from pressure forces distributed all along the body. The term buoyancy is used because the force is generated by a pressure distribution. (A related example of buoyancy force is the additional thrust or drag on a body caused by a nonuniform cross-sectional area in a wind tunnel.) For the case of zero propeller thrust, the solid streamlines in Fig. 5, the buoyancy thrust is also zero. As thrust is increased, the change to the dashed lines of Fig. 5 causes a pressure distribution change which gives the buoyancy force.

Direct calculation of the buoyancy force would be very difficult. A better way is to consider the energy and momentum in the inviscid flow of all the stream tubes affected by the propeller. When the propeller thrust is increased from zero to some positive value, the airspeed at the propeller plane is increased from $V_1(r)$ to $V_2(r)$, where $V_2(r) = [1 + a(r)]V_1(r)$.

In order to calculate $a(r)$ and the blade forces for each stream tube, we use the approximation that radial forces and velocities may be neglected. This is the same approximation used for the propeller in a freestream, but the addition of the airframe changes the radial velocity distribution. The appendix method is used to calculate blade forces as before, giving T_P.

For the propeller alone in a freestream, the speed $V_1(r)$ becomes the same as the freestream speed V_0. A consideration of the conservation of momentum and energy along a streamtube shows that the speed $V_3(r)$ far downstream is related to $V_1(r)$ by $V_3(r) = [1 + 2\,a(r)]V_1(r)$.

When the body interference is added to the problem and thrust is produced, making $a(r)$ greater than zero, the speed far downstream may be shown to be

$$V_4(r) = \{V_0^2 + 4a(r)[1 + a(r)][V_1^2(r)]\}^{1/2} \qquad (6)$$

The interference causes $V_4(r)$ to be different from $V_3(r)$. The speed $V_2(r)$ is the airspeed at the propeller. The speed $V_1(r)$ is used in the Appendix for calculating $a(r)$ and the propeller blade forces. In all of the above, r refers to the stream tube which passes the propeller plane at distance r from the propeller centerline.

The factor $a(r)$ is used to calculate the ratio $T_R(r)$ of the total thrust to the propeller thrust for each of the stream tubes. The ratio is

$$T_R(r) = \frac{V_4(r) - V_0}{V_3(r) - V_1(r)} = \frac{\{1 + 4a(r)[1 + a(r)]V_{10}^2(r)\}^{1/2} - 1}{2a(r)V_{10}(r)} \qquad (7)$$

where $V_{10}(r) = V_1(r)/V_0$. The thrust ratio, $T_R(r)$, is approximately equal to $V_{10}(r)$ for typical values of $a(r)$, which are near 0.1. For example, if $V_{10}(r)$ is 0.91 (a typical value for the Luscombe), then $T_R(r)$ is near 0.92, and the propeller thrust of the stream tube is about 1.08 times the total thrust. Then the buoyancy force is a drag that is 0.08 times the total thrust. If $V_{10}(r)$ is greater than 1, $T_R(r)$ is greater than 1, and the stream tube generates buoyancy thrust.

Equation (7) is used in a program to integrate the stream tubes over the propeller plane to obtain the propeller thrust T_P, the total thrust T, the buoyancy thrust T_B, and the propeller torque Q. These parameters are used with the rotational speed Ω to find the propeller efficiency, defined as

$$\eta = (TV_0/\Omega Q) \qquad (8)$$

A natural tendency is to define the efficiency using T_P in place of T, and then accounting for T_B separately. If this were done, we could cite cases where $V_{10}(r)$ is small enough that η would be greater than 1.0. But since both T_P and T_B are generated by propeller rotation, and since use of Eq. (8) involves blade friction and momentum losses, η has been defined using T, and hence, η must always be less than 1.0.

Next, consider the viscous effects in the body boundary layer of Fig. 5. As the propeller thrust is increased from zero to some positive value, drag is increased from several effects, namely 1) scrubbing drag, 2) separation drag, and 3) cooling drag.

The "scrubbing" drag is that caused by the airspeed increase over the fuselage or other parts, both from the increased axial speed of the slipstream and from crossflow velocities caused by the propeller rotation. The separation of the airflow and the static pressure distribution near the downstream end of the body may be altered by the thrust increase. The increase may also increase the drag of airflow through engine cooling ducts, since at zero thrust the doors (if present) to the ducts may be closed, but the doors should be opened as thrust is increased.

These drag effects can hardly be measured directly, but they are very important to aircraft performance. They are the difference between drag in powered flight and drag in gliding flight! Since the former can be obtained using propeller calculations, and the latter from zero-thrust testing, the sum of these important drag effects can be obtained.

The viscous interaction between the propeller flow and the airframe causes some small but unknown modification of the buoyancy force on the airframe. To correct the situation, the authors recommend that the body buoyancy force be defined as given above, assuming the ideal, inviscid case. Then the total thrust can be calculated as shown in this article. The difference between this idealized buoyancy thrust and the "real" buoyancy thrust can be accounted for by defining it as a part of the viscous drag effects.

The viscous effect on buoyancy thrust makes the distinction between thrust and drag less clear, but the important factor for airplane performance calculations, the difference $T - D$, as used in Eq. (1), remains unchanged.

Drag and Propulsive Efficiency of the Luscombe 8E Aircraft

Drag, propulsive efficiency, and many other parameters have been calculated using the data in Tables 1 and 2 in a computer program. The program makes use of Eqs. (1–8), plus the propeller relations and iteration procedure given in the Appendix. The Luscombe has a span $b = 34.5$ ft (10.52 m), and a wing area, $S = 140$ ft^2 (13.01 m^2), so that $AR = 8.5$. The wing chord is constant except for some tapering near the tips and two wing root cutouts in the trailing edge (see Fig. 1). Each cutout extends forward from the trailing edge about 1 ft, and spans about 1 ft. The wing has a NACA 4412 airfoil. The airplane has a Continental C85-12F engine with a maximum rating of 85 hp. This drives a McCauley, two-bladed 71-in. (1.803-m) diam propeller with a 51-in. (1.295 m) pitch. Table 3 gives blade information (used in the program) as a function of the radius from the crankshaft centerline. A flat-bottom RAF6 airfoil is used on the blades. Blade angles were measured with respect to the flat, lower surfaces of the airfoils.

During a typical computer run, the computer finds the angle of attack at each of the above nine blade elements, calculates the lift and drag coefficients and the induced velocity param-

Table 3 Propeller data

Radius, in.	Chord, in.	Blade angle, deg	Thickness ratio
13.300	5.20	30.15	0.154
16.075	5.24	25.45	0.130
18.850	5.17	22.25	0.114
21.625	5.00	19.85	0.100
24.400	4.76	18.05	0.089
27.175	4.44	16.52	0.081
29.950	3.92	15.08	0.076
32.725	3.30	13.92	0.072
35.500	2.60	12.81	0.069

eters at each element, and uses an integration routine to sum the total forces and moments on each blade from radii of 13.3 to the tip at 35.5 in. No explicit account has been taken of the propeller forces inboard of 13.3 in., as the blade cross section rapidly becomes a structural shape and has little thrust in this region. The RAF6 section drag coefficient used in the appendix is a little larger than expected for this airfoil in order to roughly compensate for the drag effects of the inner region.

No suitable RAF6 airfoil test data was available, so estimates of this data were made using Ref. 8. To simplify matters, the airfoil zero-lift angle was taken to be constant all along the blades. We will say more about this constant, α_0, later.

The angle of attack of the fuselage reference line was estimated to be

$$\alpha = C_L/0.0814 - 3.64 \tag{9}$$

in degrees, and the engine was mounted with 1.43 deg of downthrust. Therefore, the propeller plane was almost perpendicular to the freestream for C_L values near 0.4, but for the larger values of C_L the freestream is several degrees away from being perpendicular. This means that the down-going blade has its angle of attack increased by some amount, but since the up-going blade has its angle decreased, the two effects tend to compensate for each other. No account of this phenomenon was used in the program.

Since α_0 was not accurately known, and since α_0 has such a direct effect on the blade lift forces [see Eq. (A9)], the value of α_0 was adjusted to cause the program to match the zero-thrust calibration point. The required value, -4.8 deg, was used for both glide and level flight determinations of drag.

The lift curve slope in Eq. (A9), $C_{L\alpha}$, was taken to be 0.100/deg, based on Ref. 8 and other airfoil data. $C_{L\alpha}$ is almost constant for various airfoil shapes. Its value has essentially zero effect on glide results, but level flight thrust levels are almost directly proportional to $C_{L\alpha}$.

The other parameter that has a significant effect on the thrust output of the program is the airflow slowdown factor u_s. Program sensitivity to this parameter was the reason that special care was taken to not overlook any phenomena that contribute to u_s.

For gliding speeds significantly larger than that for which the crankshaft was level, the computer program showed that about 1 lb of negative thrust was developed. This came about because the higher airspeeds, which had lower values of C_L and angle of attack, also had a slightly smaller u_s as shown on Fig. 3. The u_s change caused the negative thrust. This does not cause an error in the drag values determined, inasmuch as Eq. (1) is used by the program to separate the thrust and drag effects. The effect of the change in u_s is so small that it can be ignored for most purposes.

The program was used to determine C_{DG} as a function of C_L, which is shown by the circular points on Fig. 6. The points are closely matched by the empirical relation

$$C_{DEQ} = 0.0325 + 0.009444(C_L - 0.4)^2 + C_L^2/(\pi ARe) \tag{10}$$

where $e = 0.74$. The 0.009444 term is used to model the variation of wing NACA 4412 profile drag data with changes in C_L. Hence, Eq. (10) indicates that the Luscombe 8E wing has an Ozwald efficiency factor $e = 0.74$, and Eq. (10) is plotted as a solid line on Fig. 6. Both the figure and Table 4 show that the differences between C_{DG} and C_{DEQ} are small.

The Ozwald efficiency factor may be lower than might otherwise be expected because of losses from leaks around the ailerons, including those from the corrugated construction of the trailing edges, and because of the wing cutouts.

The triangular data points on Fig. 6 represent C_{DEP} as determined by the first method, the measurement of engine power. These points are well-matched by a solid line, which represents the second method for finding C_{DEP}. That is, the program calculates C_{DEP} based on propeller geometry, rpm, atmospheric density, etc. Note that the good agreement of these methods gives a vote of confidence on the estimate of a value for $C_{L\alpha}$. Note also that these two methods are independent of the glide data results, except that the second method uses the airfoil parameter α_0 found in the glide testing.

The second method also computes the propeller efficiency, given by Eq. (8). The efficiency is used to determine C_{DL} on Fig. 6, since

$$C_{DL} = \eta C_{DEP} \tag{11}$$

C_{DL} is shown on Fig. 6 both as the square points and the solid line.

No data points are shown for the first method for C_L greater than 0.6. This is because the engine charts cover only shaft speeds of 1800 rpm and higher. An extrapolation of the charts to lower rpm failed to produce data that matched the second method.

The glide, the level flight, and the engine power data shown on Fig. 6 were used to calculate the drag vs airspeed data given in Fig. 7. The symbols and solid lines on Fig. 7 corre-

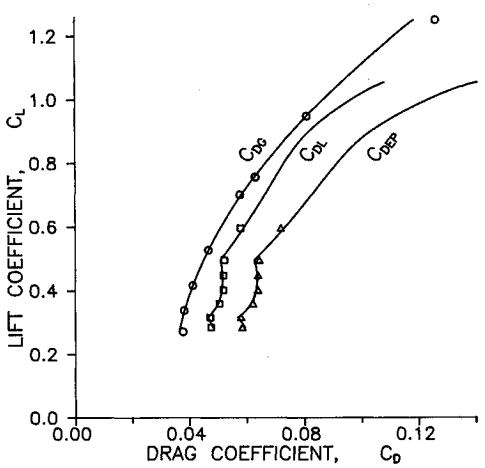

Fig. 6 Luscombe 8E gliding, level flight, and engine power drag coefficients vs lift coefficient.

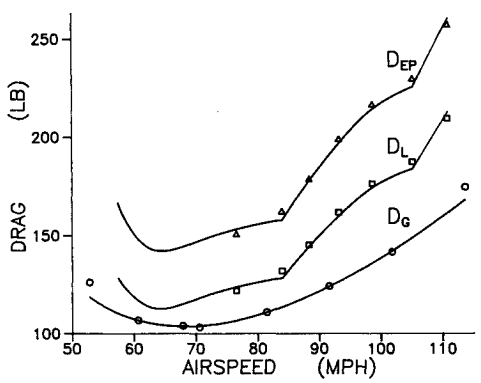

Fig. 7 Luscombe 8E gliding, level flight, and engine power drag values vs equivalent airspeed for 1250-lb weight.

Table 4 C_{DG} minus C_{DEQ}

C_L	0.2704	0.3370	0.4156	0.5267	0.7009	0.7566	0.9479
$C_{DG} - C_{DEQ}$	0.0014	−0.0002	0.0000	0.0000	0.0005	−0.0003	0.0000

Table 5 Luscombe 8E flight efficiency factors for 1250-lb weight at sea level conditions with revisions for open cooling ducts in the glide

Airspeed, mph	60	70	80	90	100
Lift coefficient	0.970	0.713	0.546	0.431	0.349
Level flight efficiency, η_L	0.936	0.879	0.867	0.813	0.784
Propeller efficiency, η	0.781	0.802	0.810	0.812	0.813
Propulsive efficiency, η_P	0.731	0.705	0.703	0.660	0.638
$a(r = 18.85$ in.)	0.175	0.129	0.115	0.102	0.096
$a(r = 29.95$ in.)	0.190	0.162	0.130	0.117	0.102
Revised η_L	0.912	0.846	0.827	0.770	0.740
Revised η_P	0.712	0.678	0.670	0.625	0.602

spond to those on Fig. 6. The calculations were done for sea level conditions and an airplane weight of 1250 lb.

The corresponding level flight, propeller, and propulsive efficiency factors are given in Table 5 as a function of airspeed and lift coefficient. The table also gives the streamwise induced velocity factor a at two radial locations along the blades.

The Luscombe was designed without doors to block engine cooling airflow when less air is needed, as in gliding flight. Hence the gliding drag values in Figs. 6 and 7 are larger than needed for gliding flight by the amount of the cooling drag. The engine cooling airflow, which emerges from an opening about 5-in. (127-mm) long by 20-in. (508-mm) wide in the underside of the engine cowling, is estimated to increase the airplane drag area by approximately 0.3 ft^2 (0.0279 m^2). This area has been used to calculate a revision to the drag coefficient curve in Fig. 6, and from this revised values of η_L and η_P, as given in Table 5. The change reduces the propulsive efficiency for cruising at 90 mph from 0.660 to 0.625. This brings the propulsive efficiency closer to that of the Bellanca in cruise, about 0.58.[1] Note that the Bellanca was tested with the inlet and outlet ducts sealed. The revised values are more representative of the true propulsive efficiency, which should account for all engine installation effects. Zero-thrust testing can be done for aircraft with closable doors on the cooling ducts. The drag effects of closing the doors should be enlightening.

The propulsive efficiency of the Luscombe decreases markedly with increasing airspeed, a significant finding. Similar decreases were recorded from the Bellanca testing.

The ratio of propeller thrust to total thrust on the Luscombe is very close to 108% for all airspeeds. In other words, there is a buoyancy drag force on the airframe that is 8% of the total thrust.

Current Flight Testing

The Comparative Aircraft Flight Efficiency (CAFE) group of Santa Rosa, California is in the process of using the zero-thrust testing method. CAFE has been developing a boom for attachment to various aircraft for accurate measurement and automatic recording of airspeeds, temperatures, pressure altitudes, and other flight data. They are working with the Experimental Aircraft Association to test a number of private aircraft per year, and plan to publish drag and propulsive efficiency results.

Conclusions

1) The zero-thrust glide-test method provides the first practical, accurate, and economical means of measuring glide drag and propulsive efficiency as a function of speed on propeller aircraft. The glide drag versus airspeed curve enables one to determine an "Ozwald" wing efficiency factor as well as a zero-lift drag level.

2) The zero-thrust sensor provides a basis for an accurate propeller analysis for calculating propeller efficiency, thrust, and hence drag in level flight.

3) The propulsive efficiency of the Luscombe 8E, a typical, two-place tractor aircraft, has been found to be near 62% at a cruising speed of 90 mph (40.2 m/s), in spite of a propeller efficiency of over 81%. That is, the ratio of level flight drag to gliding drag is 1.30. Such losses from the interaction of the propeller slipstream with the aircraft are believed to be typical of many propeller aircraft.

4) The above numbers are based on the engine cooling ducts being closed during the glide. The added drag of opening the ducts during the glide gives an apparent propulsive efficiency that is larger than the above.

5) A buoyancy thrust (or drag) is generated on the airflame as a result of the interference between the propeller flow and the airflame flowfields. A method has been developed for finding the buoyancy force. This is a drag of 8% of the total thrust on the Luscombe 8E.

Appendix: Computing Method for Propeller Thrust and Power Calculations

The force coefficients in Fig. 4 are resolved into the thrust direction as C_Y and in the propeller plane direction, representing torque, as C_X. Then we have

$$C_Y = C_\ell \cos\phi - C_d \sin\phi \tag{A1}$$

$$C_X = C_\ell \sin\phi + C_d \cos\phi \tag{A2}$$

We can then write the relations equating the blade element forces to the mass flow rate of the airstream times the speed increases of the airstream. Here V is understood to be the stream airspeed, which is the same as the airspeed $V_1(r)$ used in the main part of this article. Also, a is the same as $a(r)$ used in the main part of this article. We know from momentum theory[7] that the air speeds up by the factor $(1 + a)$ in passing through the propeller disk area, and that far downstream the air speed is $(1 + 2a)V$. Then the thrust T per unit radius of the propeller blades is

$$\frac{dT}{dr} = C_Y\left(\frac{\rho}{2}\right)\left[\frac{(1+a)V}{\sin\phi}\right]^2 Bc$$
$$= \rho(1+a)V(2\pi r)(2aV)F \tag{A3}$$

where B is the number of blades and c is the blade chord length. Q is the propeller torque, and the corresponding torque relation is

$$\frac{1}{r}\frac{dQ}{dr} = C_x\left(\frac{\rho}{2}\right)\left[\frac{(1+a)V}{\sin\phi}\right]^2 Bc$$
$$= \rho(1+a)V(2\pi r)(2a'\Omega r)F \tag{A4}$$

The factor F in the above is Glauert's blade interference factor, which is defined by

$$F = \frac{2}{\pi}\cos^{-1}\left\{\exp\left[-\frac{B}{2\lambda}(1+\lambda^2)^{1/2}\left(1-\frac{r}{R}\right)\right]\right\} \tag{A5}$$

where

$$\lambda = (V/\Omega R) \tag{A6}$$

Referring again to Fig. 4, we see that

$$\phi = \tan^{-1}[(1+a)V/(1-a')r\Omega] \tag{A7}$$

Also

$$\phi = \beta - \alpha \tag{A8}$$

Now, the problem is to solve the four Eqs. (A3), (A4), (A7), and (A8) for the four unknowns α, ϕ, a, and a'. This is done at each station of interest along the blade radius so that the forces may be integrated to obtain the total thrust, torque, and power input to the propeller.

The computer program uses an iterative procedure to find the solution at each blade element of interest. Step 1 is to

guess the value of α, and then find ϕ from Eq. (A8). Then the method solves for a, a', and finally a second value of ϕ using Eq. (A7). If the second value is not equal to the first value, the procedure is repeated using a new value of α. The procedure is repeated until the two values of ϕ are equal, and a solution is attained.

The details of the procedure after step 1 are the following: step 2 is to use (A8) to find ϕ. Step 3 is to find C_ℓ and C_d from aerodynamic data on the blade airfoil. The airfoil basic lift coefficient C_1 is given by

$$C_1 = 0.1(\alpha - \alpha_0) \tag{A9}$$

The basic lift coefficient was then modified to limit its maximum value to 1.5. The modified and final lift coefficient is given by

$$C_\ell = \{1.5 + C_1 - [(1.5 - C_1)^2 + 0.04]^{1/2}\}/2 \tag{A10}$$

and the section drag coefficient by

$$C_d = 0.015 + 0.03[(4C_1/3) - 1]^4 \tag{A11}$$

Step 4 is to compute the Prandtl tip loss correction factor, given by Eq. (A5). Step 5 is to use Eqs. (A1) and (A2) to calculate C_Y and C_X. Step 6 is to calculate the section solidity factor σ from

$$\sigma = (Bc/2\pi r) \tag{A12}$$

Step 7 is to calculate a and a' by using Eqs. (A13–A16). These relations can be obtained using Eqs. (A3), (A4), and (A7).

$$K_F = (C_Y/4F \sin^2\phi) \tag{A13}$$

$$K'_F = (C_X/4F \sin\phi \cos\phi) \tag{A14}$$

$$a = [\sigma K_F/(1 - \sigma K_F)] \tag{A15}$$

$$a' = [\sigma K'_F/(1 + \sigma K'_F)] \tag{A16}$$

Step 8 is to use Eqs. (A7) and (A8) to find new values for ϕ and α. This completes the iteration procedure.

The computer uses an integration procedure to sum the forces on the propeller blades to obtain propeller torque, direct propeller thrust, and the total thrust.

References

[1]Raspet, A., and Lambros, G., "Flight Research on a Personal Type of Airplane," *Research Reviews*, Office of Naval Research, Dept. of the Navy, Washington, DC, April 1954.

[2]Johnson, R. H., "Sailplane Flight-Test Performance Measurement," *Journal of the Soaring Society of America*, April 1968, pp. 10–16.

[3]Johnson, R. H., "A Flight Test Evaluation of the AS-W22," *Journal of the Soaring Society of America*, April 1983, pp. 22–30.

[4]Glauert, H., "Airplane Propellers," Vol. IV, Division L, *Aerodynamic Theory*, W. F. Durand, 1934.

[5]Larrabee, E. E., "Propeller Design for Motorsoarers," NASA CR 2085, Jan. 1979, pp. 285–303.

[6]Larrabee, E. E., "Propeller Design and Analysis," National Free Flight Society, International Symposium Rept., San Jose, CA, 1979, pp. 9–26.

[7]Adkins, C. N., and Liebeck, R. H., "Design of Optimum Propellers," AIAA Paper 83-0190, Jan. 1983.

[8]Abbott, I. H., and Von Doenhoff, A. E., *Theory of Wing Sections*, Dover, New York, 1959, Appendix IV, pp. 360–390.